Structural Eng./Earthquake Eng., JSCE, Vol. 18, No. 1, 13s－25s, 2001 January
(J. Struct. Mech. Earthquake Eng., JSCE, No. 668/ I－54)

FATIGUE PERFORMANCE OF BUTT-WELDED JOINTS CONTAINING VARIOUS EMBEDDED DEFECTS

Chitoshi MIKI[1], Fauzri FAHIMUDDIN[2] and Kengo ANAMI[3]

[1]Fellow of JSCE, Dr. of Eng., Professor, Dept. of Civil Eng., Tokyo Institute of Technology,
(12-1 Ookayama 2 chome, Meguro-ku, Tokyo 152-8552, Japan)
[2]Graduate Student, Dept. of Civil Eng., Tokyo Institute of Technology,
[3]Member of JSCE, Research Associate, Dept. of Civil Eng., Tokyo Institute of Technology,

The presence of possible welding defects needs to be taken into account in order to get rational performance of welded structural member considering its fitness for purpose. Accordingly, it is necessary to identify fatigue performance of welded joint containing various defects. Fatigue performance of butt-welded joint specimens considering five types of defect, which are vary in size and location, is studied in wider fatigue life range. It is observed that the shape, size, and location of the defects considerably affect the fatigue performance of the specimens. Fatigue life prediction by fracture mechanics analysis based on current recommendation is generally conservative in long life region.

Key Words : *fatigue, butt-welded joint, weld-defect, embedded-defect, defect-size, defect-location*

1. INTRODUCTION

Welded joints very often include embedded defects. Those defects are, such as, cracks, lack-of-fusion, incomplete-penetration, blowhole, porosity, slag-inclusions and similar discontinuities[1)-3)]. All of the defects may reduce fatigue strength of the welded joints[4)-8)]. Fatigue performance of welded joints containing defects may vary in type, size, shape, location of defects, and also geometry of the joints. Many studies on the effects of the presence of weld defects to the fatigue strength were carried out. Ishii et al[9)] found that the presence of crack, undercut, and incomplete-penetration in steel welded joints had a great effect of lowering the fatigue strength. Ishii and Iida[10)] examined fatigue behavior of various defective butt welds specimens. It was reported that weld defect severity, which was defined as ratio of weld defects to the areas of fracture surface, are dominant influencing factor on fatigue strength of the defective butt welds, as well as, the length of weld defect. Furthermore, Newman and Gurney[11)] reported that the depth of weld defect was a significant variable in determining fatigue strength. Effect of porosity, slag inclusion, and blowhole defects were reported by Harrison[12),13)] and Miki et al [14),15)], respectively.

It is obvious that the presence of defects is not expected, however, to repair perfectly all of the defects is sometimes difficult and also costly[8)-16)]. It is therefore important to introduce the concept of "permissible defects" in design, fabrication, and inspection, as well as, necessary to establish the rational acceptance criteria based on the fitness-for-purpose of the components or structures[17)-18)]. When the defect is detected, it should be decided whether repair is necessary or not.

To assess the harmfulness of weld defects, some recommendations, for example IIW[19)], WES 2805-1997[20)], and JSSC-1995[21)], recommend to apply fracture mechanics analysis in terms of fatigue propagation life. There are some assumptions have been made, such as, initial crack shape.

The defects are generally classified as volumetric and planar types. It has been assumed in fracture mechanics analysis that the volumetric defect can be assessed on the basis of the same dimension as planar one with an overly conservative result[5)-22)]. This study is intended to examine sensitivity of each type of defect on fatigue performance of butt-welded joints containing typical embedded defects, both volumetric and planar. In addition, permissible defect size is evaluated from the discussion of the sensitivity of the embedded defects.

2. SPECIMENS

Specimens used in this study were made of JIS SM490A steel plates with 25-mm thick. The

Table 1 Chemical composition and mechanical properties of base metal from JIS SM490A, 25mm thick

C %	Si %	Mn %	P %	S %	Y P MPa	T S MPa	El. %
0.17	0.44	1.44	0.013	0.006	343	532	33

Table 2 Chemical composition and mechanical properties of deposit metal from DW-Z100

C %	Si %	Mn %	P %	S %	Cu %	Y P MPa	T S MPa	El. %	VEo J
0.03	0.52	1.50	0.013	0.008	0.01	497	567	28	153

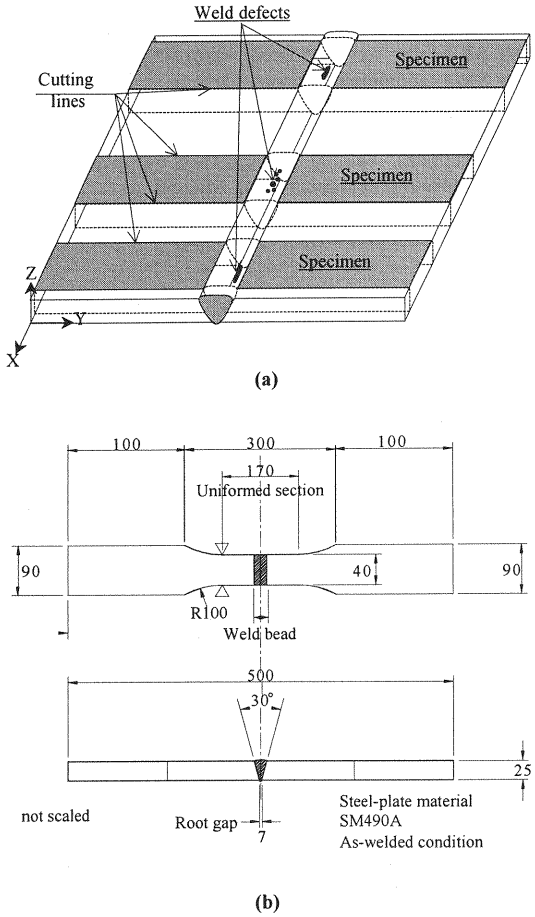

Fig.1 Specimens preparation and configuration

chemical composition and mechanical properties of the plate are shown in **Table 1**. The specimens were fabricated by applying CO_2 gas shielded arc welding process using multipass weld method with single Vee (V) groove shape. This type groove is commonly used for the butt weld joints of flange

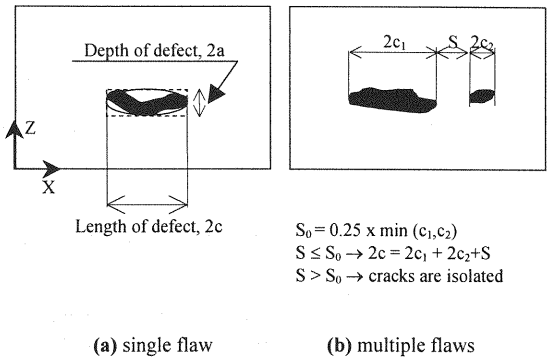

Fig.2 Illustration of defect length and depth

plate, which are welded in site. The number of welding pass is varied from 6 to 10 layers. The deposit metal used was DW-Z100 with wire diameter of 1.2 mm. Chemical composition and mechanical properties of the deposit metal are shown in **Table 2**.

The defects contained in specimens are crack (CR), incomplete-penetration (IP), lack-of-fusion (LOF), slag-inclusion (SI), and blowhole (BH), which are vary in size and location. The CR type defect installed in this study is weld hot crack. This kind of crack type defect often occurs in first layer of multipass welding. For this reason CR type defect in this study was installed in the first layer. Similarly, IP type defect was also installed in the first layer. As to other types of defect, they were installed around center of the welded cross section.

The fabrication of specimens was conducted in following steps. First, a pair of wide plates was connected, which include various embedded defects that are varying in size and location. After the plates have been completely connected, the welded joints were then examined by applying Radiographic Testing (RT) following JIS Z-3104 procedure with A-level of image quality. If any defects were detected, cutting lines were then determined to be prepared as a specimen. The defects are located at about the center of specimen, as shown in **Fig.1(a)**. After cutting, the location and size of defects were once more examined by using manual Ultrasonic Test (UT) which comply with JIS Z-3060. The shape and dimensions of specimens are shown in **Fig.1(b)**.

To assure that weld defect would dominantly control fatigue crack initiation the cut edges were smoothly finished. The weld surfaces are kept in as-welded condition.

There were 150 joint specimens prepared for this study, which consist of 30 specimens for the each type of defect.

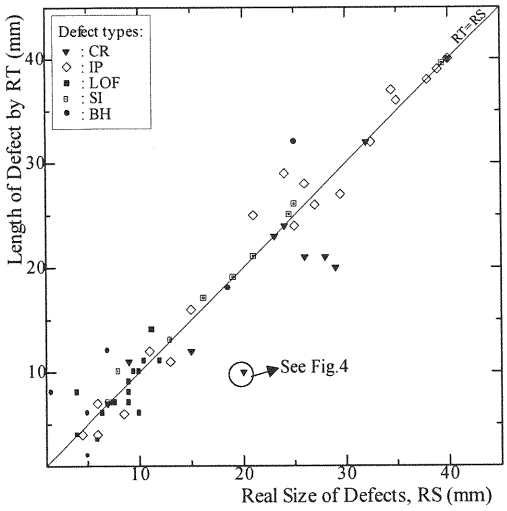

Fig.3 Comparison between RT and Real Size

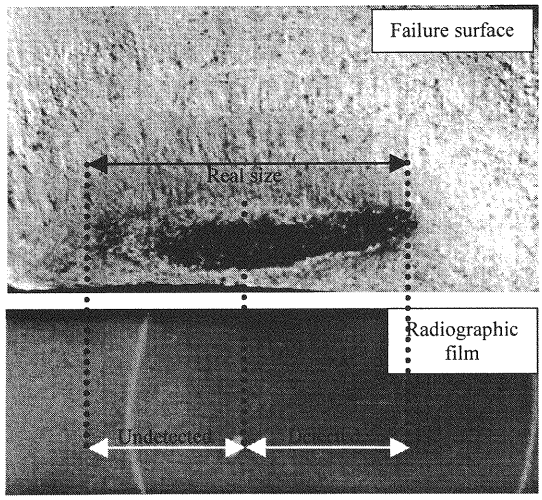

Fig.4 RT result and real size of specimen CR-9

In this study the defect length, called 2c, is used as the representative size of defect shown in **Fig.2**. The depth of defect is almost impossible to be detected by RT. Therefore, only length is used to indicate size of defect. To decide the length of defect consisting of multiple defects, the method for defining interaction of multiple planar defects recommended in WES 2805[19] is followed, as shown in **Fig.2(b)**. It depends on the distance between adjacent crack tips.

In order to evaluate the results of RT, the lengths of defects on failure surfaces were measured after fatigue test. These measured results called as real size is compared with the RT results, as shown in **Fig.3**. Some specimens with CR type defect show a wide scatter, particularly for the defects with longer size, such as 20mm length or more. It caused by the projection shape of CR defect on radiographic film that is much thinner compare to other types. In addition, the projection along the defect length may have different shape. One part can be closed, while other part is a little bit distantly spaced. Therefore, it is difficult to detect, and some part of the defect length can not be recorded on the radiographic film. One of the cases is shown by specimen CR-9, as performed in **Fig.4.** The real size of this defect is about two times larger than the size resulted by RT, as marked by circle on the plot data in **Fig.3**.

Specimens containing BH type defect show relatively scattering result. It is due to the defect condition that consists of plural numbers of blowholes. By using RT, this group of defects is imaged as one defect. On the other hand, the location of defects is sometimes scattered, and may be treated as a smaller size of defect. Therefore, this defect type tends to have over estimated defect size based on RT result.

For specimens with IP and LOF defects, the results show a closed agreement between real size and RT results. Specimens containing SI defect particularly shows a very closed agreement. It is because the shape of this defect is generally thicker in compare with other defects.

As for small size defects, the results are relatively scattered compared with larger size defects. This is caused by the ability of the equipment, which is generally more difficult at detecting small size defect.

3. FATIGUE TEST RESULTS AND OBSERVATION OF FAILURE SURFACES

The fatigue tests were carried out under constant stress ranges. The stress ratio, R, was about 0, and the stress ranges were varied from 100 to 350 MPa. In case of specimens that were unbroken in lower stress range, they were tested again by higher stress ranges, which eventually made the specimens failure.

Fatigue test results are plotted in S-N curves as shown in **Figs.(5a)** to **(5e)** representing the specimens that contain of CR, IP, LOF, SI, and BH type defects, respectively. Some of specimens failed with fatigue-cracks originated from embedded defects, and some other specimens have fatigue cracks initiated from weld-toes. The cracks from defects are indicated by open circle in the S-N

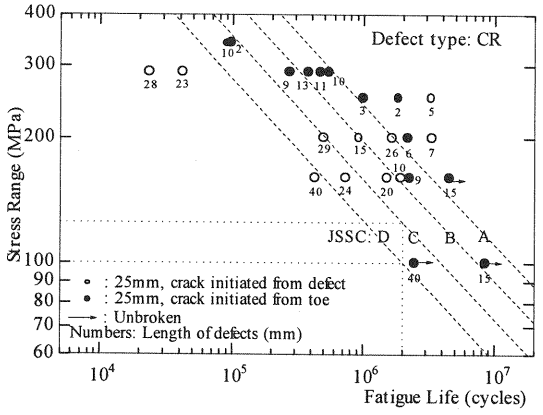

(a) S-N curve of CR type defect

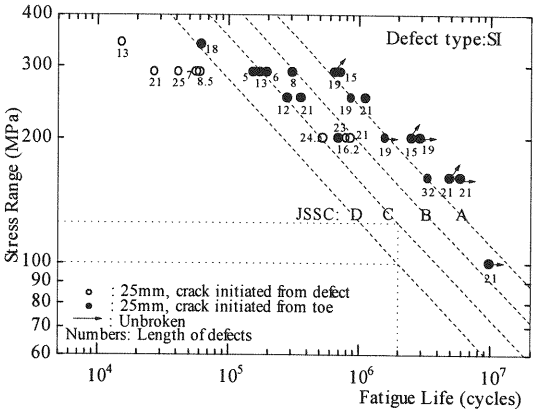

(d) S-N curve of SI type defect

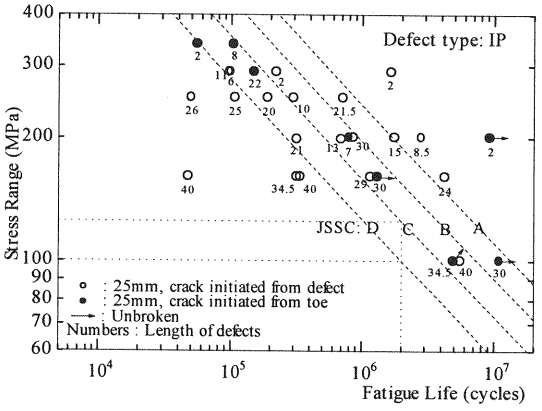

(b) S-N curve of IP type defect

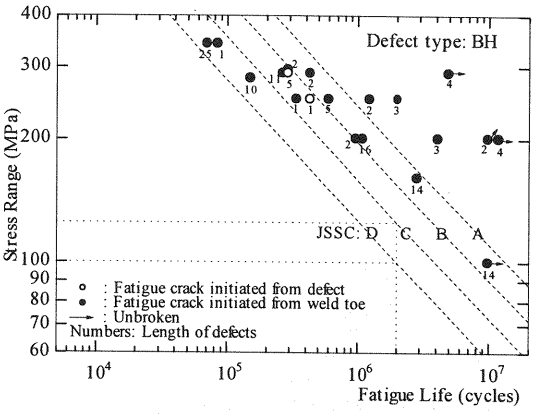

(e) S-N curve of BH type defect

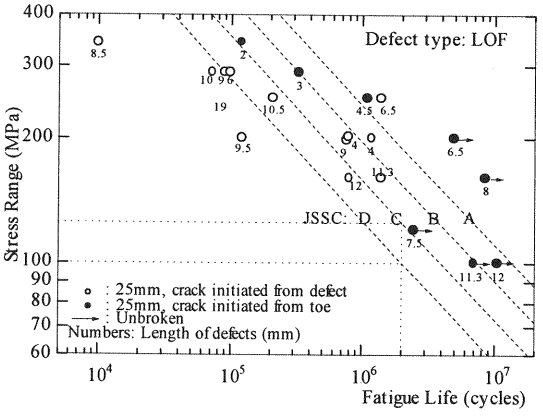

(c) S-N curve of LOF type defect

Fig.5 Fatigue test results

curves, while cracks from weld toes are indicated by solid circle. The numbers beside the symbols indicate the sizes of defect in length, 2c, as illustrated in **Fig.2**.

The length of defects measured on failure surfaces after fatigue tests is used, because real size is more suitable to evaluate the sensitivity of each type of defect. For specimens failed with the cracks from weld toes the sizes obtained by RT are used. The typical failure surfaces of specimens are shown in **Figs.6(a)** to **6(e)** representing each type of defect.

The butt-welded joints are classified as D-class fatigue strength category in the JSSC fatigue design recommendation[21]. From the results of specimens in which fatigue cracks initiated from embedded defects, although the defects are notably large, some of specimens can satisfy the fatigue strength category.

The depths of the embedded defects, called 2a, were also measured on the failure surfaces following

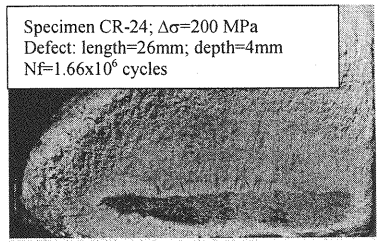

(a) Failure surface of specimen with CR type defect

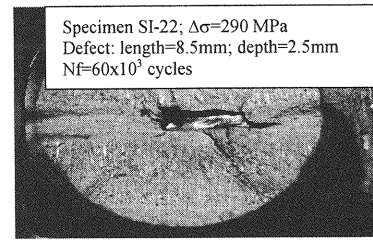

(d) Failure surface of specimen with SI type defect

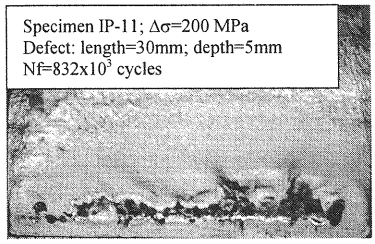

(b) Failure surface of specimen with IP type defect

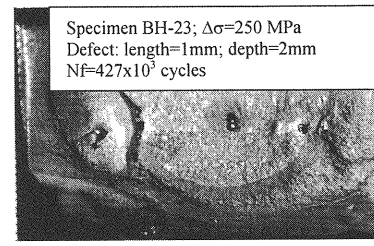

(e) Failure surfaces of specimen with BH type defect

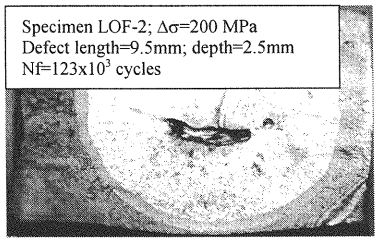

(c) Failure surface of specimen with LOF type defect

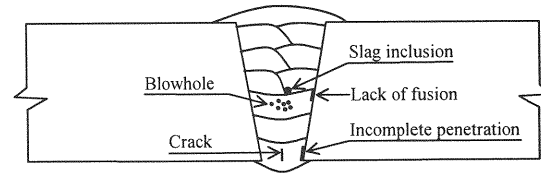

(f) Schematically illustration of defect location

Fig.6 Typical failure surfaces and location of defects

the **Fig.2**. **Fig.7** shows the aspect ratio of defect, a/c, and the length of defect, 2c. The aspect ratio decreases with the increasing of defect length and these of relatively larger defects are lower, below 0.3.

As shown by the S-N curve in **Fig.5,** some of CR and IP specimens with large defect size have high fatigue strength. The CR-24 specimen shown in **Fig.6(a)** included a crack of 26mm length was tested under nominal stress range of 200 MPa, and performs a very high fatigue strength that is plotted nearly the A-class design curve. Similarly, specimen IP-11 containing defect of 30mm performs high fatigue strength with the significantly large defect size shown in **Fig.6(b)**.

Conversely, fatigue test result of specimens containing LOF defect indicated that the same fatigue strength category can be satisfied by this type of specimen with smaller size of defects. LOF defect is located at about center of weld, as shown in **Fig.6(c)**.

As can be seen in **Fig.5(d)**, specimens with SI defect tend to fail with fatigue cracks initiated from

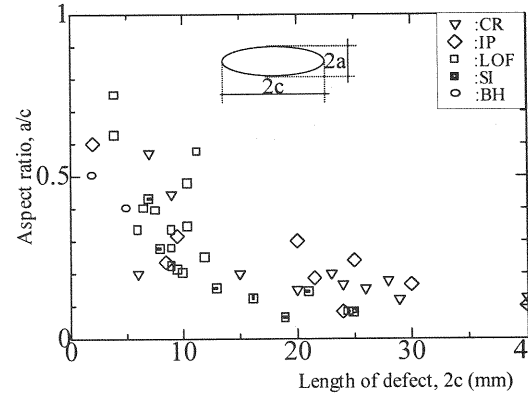

Fig.7 Defect length and its aspect ratio

the weld toes. Specimens failed with fatigue cracks initiated from defects mostly have the fatigue strength of over the C-class with significantly large defect sizes. A failure surface of specimen with this defect is shown in **Fig.6(d)**, where the defect is located near center.

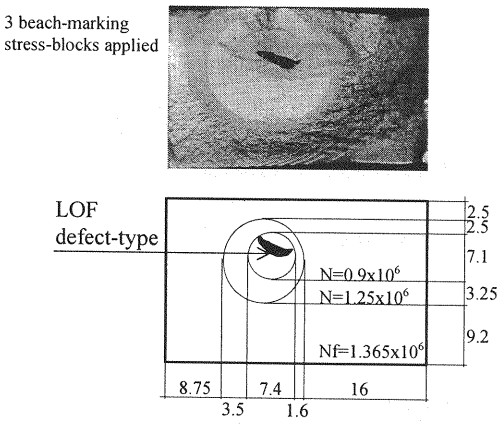

(a) Failure surface of specimen LOF-14 with beach-marks

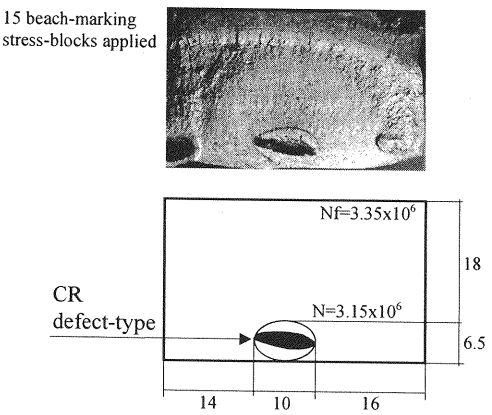

(b) Failure surface of specimen CR-1 with beach-marks

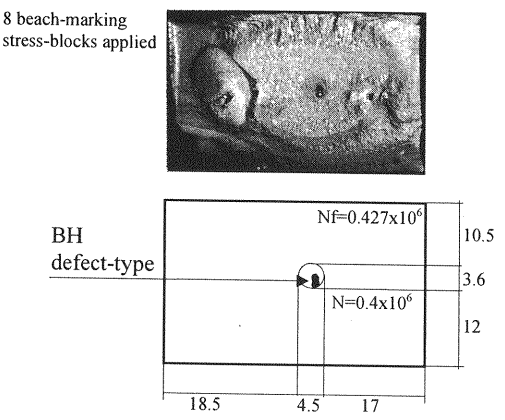

(c) Failure surface of specimen BH-23 with beach-marks

Fig.8 Schematic of failure surface with beach-marks

Fig.5(e) exhibiting the fatigue tests results of specimens with BH defect indicate that many specimens tend to fail with the fatigue cracks initiated from weld toes. Specimens failed with fatigue cracks initiated from embedded defects have fatigue strength of over the C-class.

Fatigue strength of welded joints containing defect is affected by the defect size, in which by increasing the size will decrease the fatigue strength. The fatigue tests results indicate that the sensitivity to fatigue depends on the type of defect. Specimens containing SI and BH or volumetric types of defect generally tend to failure from weld toe, and performed higher fatigue strength compare to specimens with LOF planar type defect, which is located at about the same area around center. Specimens containing CR and IP types of defect that are located near surface at lower bead performed higher fatigue strength compare to specimens containing LOF type defect that is located near center.

To observe the crack initiation and propagation behavior, beach-marking tests were carried out in order to leave contour line traces of the propagating crack on failure surfaces. Three failure surfaces including beach-mark contour lines are shown in **Figs. 8(a) to 8(c)**.

Fig.8(a) shows failure surface of specimen with LOF defect. On this specimen, from 3 beach-marking stress blocks applied during fatigue testing only the last 2 beach-marks revealed on the failure surface. The first beach-marking stress block that was applied just after $500x10^3$ cycles of fatigue test does not create a beach-mark. The specimen eventually failed after $1.365x10^6$ cycles.

Another example is specimen CR-1 contained crack, as shown in **Fig.8(b)**. There were 15 beach-marking stress blocks applied during fatigue testing. However, only one of the last beach-marking stress block created a beach-mark on the failure surface. This beach-mark was resulted after $3.15x10^6$ cycles fatigue life under 200 MPa stress range. It shows that fatigue life of about 90% was occupied to reach the first beach-mark. This result indicates that a very long fatigue life was spent before fatigue crack initiation.

Specimen BH-23, as shown in **Fig.8(c),** has only one beach-mark appeared on the failure surface. Eight beach-marking stress blocks were applied on this specimen during fatigue testing. The fatigue lives that have been applied up to seven beach-marking stress blocks were $0.35x10^6$ cycles. Therefore, at least 80% of fatigue lives were spent before fatigue crack initiation.

From the observation on the failure surfaces including the beach-marks, it is indicated that specimens containing embedded defects may have significant fatigue crack initiation life before fatigue cracks start to propagate.

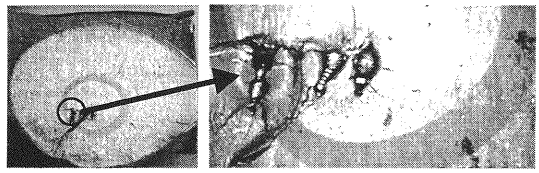

Fig.9 Multiple defects and fatigue crack initiation point

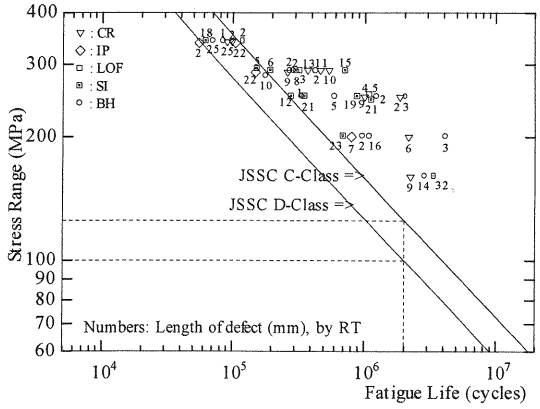

Fig.10 Summary of failure specimens with fatigue crack originated from weld toe

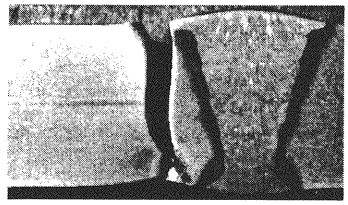

The length of the existing embedded defect, 2c = 11 mm
$\Delta\sigma$ = 290 MPa

Fig.11 Photo of fatigue crack initiated from weld toe, CR-19

In case of specimens containing multiple defects the fatigue crack generally originated from the defect with the biggest size. **Fig. 9**, as an example, shows a failure surface of specimen BH-18 having three blowholes with various sizes. There are two beach-marks revealed on the failure surface. The first beach-mark indicates that the fatigue crack initiated and propagated from the biggest defect.

Quite numbers of specimens were observed to failure with fatigue crack originated from weld toe, as summarized in **Fig.10**. As can be seen in **Fig.5,** all types of specimens indicate that weld toe can be more severe than embedded defect with smaller size than certain size of defect. One specimen failed from toe is shown in **Fig.11**. It was also observed that specimens loaded under higher stress range have a tendency to fail with fatigue crack initiation originated from weld toe.

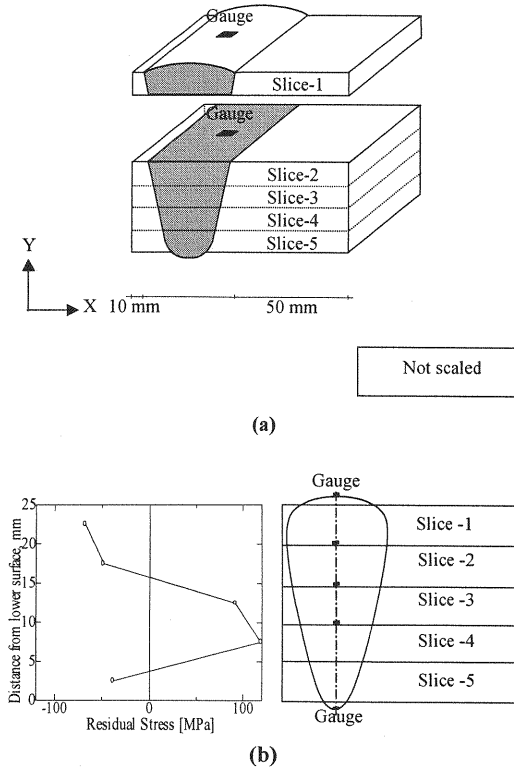

Fig.12 Residual stress distribution at weld portion

4. RESIDUAL STRESS

Residual stress distribution may affect fatigue performance of weld joints used in this study. In order to examine the residual stress distribution in the weld portion of the joint, saw-cutting method was applied. The specimens were divided into five slices. The thickness reduction is about 1.2mm for each cutting line. The reduction is taken account in the calculation. Before cutting, uniaxial strain gauge was installed at the center of weld portion on every slice to measure the strain released later after cutting. The cutting procedure was started from the upper one as shown in **Fig.12(a)**.

Fig.12(b) shows the measured result of the residual stress distribution in the X-direction through plate thickness of specimen at weld portion. It is shown that residual stress distribution at lower and upper parts are in compression, while around center part is in tension.

As illustrated schematically in **Fig.6(f),** CR and IP defects are located in the first layer of multipass welds, where the compressive welding residual stress exists. However, we can not find the clear evidence that fatigue crack is accelerated or decelerated by the residual stress from the observation of beach-marks on failure surfaces.

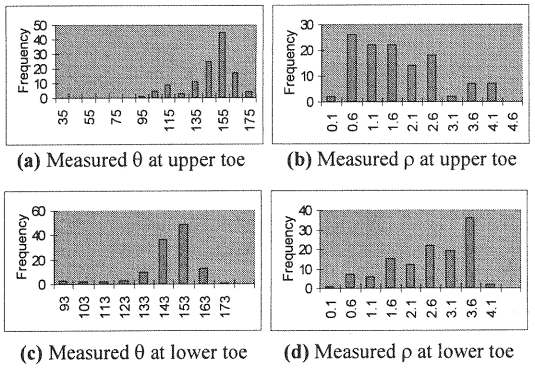

(a) Measured θ at upper toe **(b)** Measured ρ at upper toe

(c) Measured θ at lower toe **(d)** Measured ρ at lower toe

Fig.13 Histograms of measured ρ and θ at upper and lower toe

Table 3 Measurement data on weld toe

Toe	Number of Measurements	Radius, ρ (mm)			Angle, θ (degree)		
		Max	Min	Ave	Max	Min	Ave
Up.	120	4	0.1	0.7	172	95	147
Low.	120	3.8	0.1	1.2	165	35	145

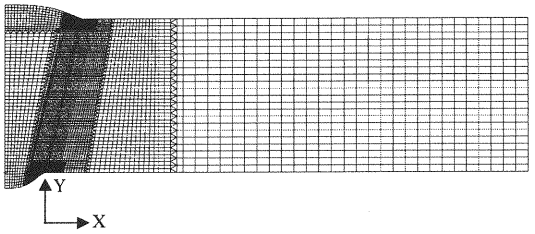

(a) FEM model of welded joint specimen

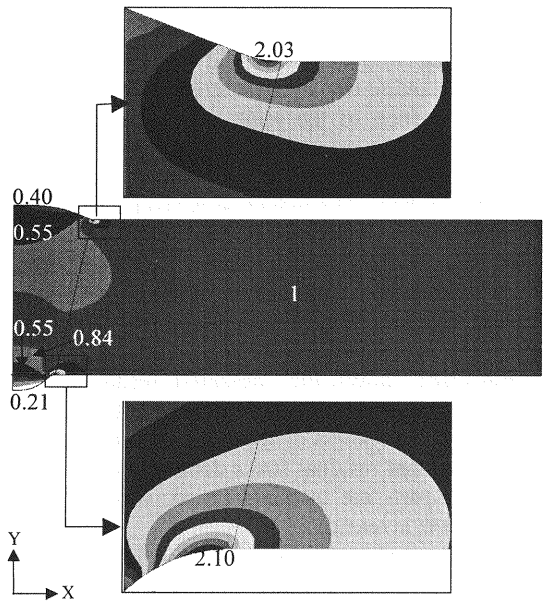

The numbers in figures indicate the stress concentration factors

(b) Stress distribution contour

Fig.14 FEM model and stress distribution contour of the joint

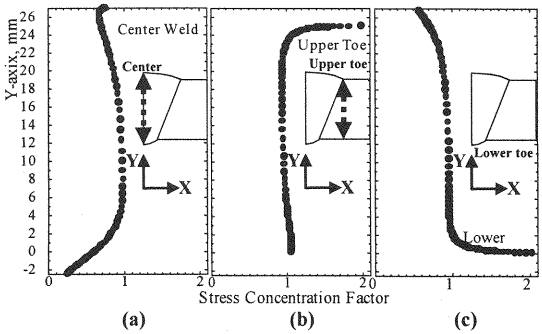

Fig.15 Stress distribution in X-direction

5. STRESS ANALYSIS BY USING FEM

(1) Stress distribution in welded joint

The locations of the weld defects are various, such as LOF, SI, and BH are located around center, but CR and IP are near lower bead. In order to explain the different of the fatigue test results between types of specimens from the viewpoint of stress field, FEM analysis was carried out.

Concerning the FEM model, local configuration of specimen was measured from some specimens. In this analysis the local radius of weld toe, ρ, and the angle, θ, and the height H and the width, W, of reinforcement both of upper and lower sides were taken from 120 measured data. The results of measurements on ρ and θ were shown in **Fig.13** and summarized in **Table 3**. Since the radii of weld toe are varied, some specimens may have very small ρ and θ at toe, while some other specimens may have an opposite situation. Therefore, in this study the critical points were observed both in upper or lower toe. In order to show general tendency of stress distribution, obtained average values of ρ, θ, H, and W were considered in the FEM model shown in **Fig.14(a).** FEM code ABAQUS was utilized and there is about 12000 of 2-D solid elements with plane strain model was used in this analysis. The minimum mesh size at weld toe is about 0.01mm.

The distribution of x-directional stress is shown in **Fig.14(b)**. The values mentioned at the figures indicate the stress concentration factor in the corresponding point. This figure shows that high stress concentration occurs at the upper and lower weld toes. The noteworthy fact that stresses in and around the upper and lower weld beads is significantly lower than the nominal stress.

Distributions of stress along the center part of weld, from upper toe through the thickness, and also from lower toe through the thickness are graphically shown in **Figs.15(a)** to **15(c)**, respectively. There is considerable decrease of stress distribution at weld

portion, and it becomes much lower at location adjacent to the surface of lower bead, where the stress distribution remains only about 21 percent. This is due to the joint geometry, especially the reinforcement. It can be said that the decrease of stress is one of the reasons why specimens containing CR and IP defects perform high fatigue strength.

(2) Crack initiation from toe

In the series of fatigue tests, fatigue failures tend to initiate from weld toe with the increasing of the applied stress ranges. The increase of the crack initiation from weld toe under higher stress range means that the weld toe becomes more severe with the increasing of the stress range compare to the embedded defect.

As listed in **Tables 1** and **2**, yield stress of base metal is 343 MPa and deposit metal used is 497 MPa. In view of this combination the specimens are overmatch joints. This overmatch may influence the tendency of the crack initiation point. In order to explain this tendency, elastoplastic analysis using plane strain model is carried out. To know the development of plastic behavior with an increase of applied stress, the average of ρ, θ, H, and W were also used. The FEM model is the same as shown in **Fig.14(a)**.

Since the weld and base metals were mixed in the joint portion, the yield stress of the mixed material become lower than the deposit metal, but higher than the base metal. Therefore, yield stress of 450 MPa is used for the mixed metal in this analysis. In the analysis, bilinear with second modulus of elasticity E' equal to E/100 is used, where $E = 2.1 \times 10^5$ MPa.

As a result of elastoplastic analysis the equivalent plastic strain distributions around the lower toe is shown in **Fig.16**. This figure performs three steps stress condition of 250, 300, and 350 MPa indicating the development of plastic strain near the toe. It is indicated by the peak plastic strain shown in the figures. The result shows that very large increase of plastic strain concentration as the load increase. However, larger plastic strain develops only in the base metal, on the contrary, very small or almost no plastic strain develops in the weld metal.

Fig.17 shows the change of cyclic stress strain behavior at the lower toe during fatigue loading with the change of applied stress amplitude. By applying the fatigue loading, repeated plastic strain occurs at weld toe. The repetition of plastic strain is one of the important factors for the occurrence of fatigue crack. This process is a local phenomenon depending on the local configuration of the toe.

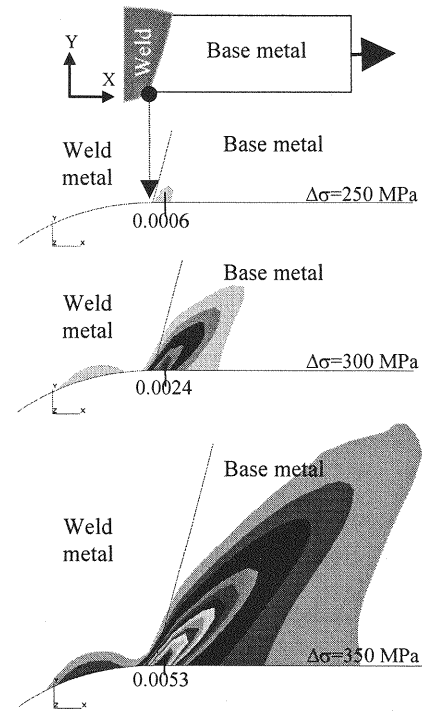

Fig.16 Equivalent plastic strain distribution around lower toe

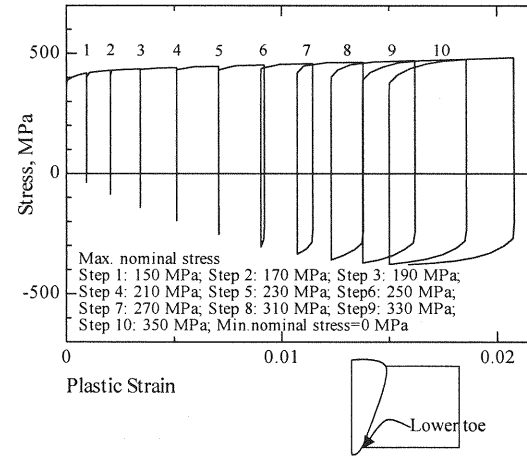

Fig.17 Stress-plastic strain relationship at lower toe

Therefore, for this analysis the minimum value of ρ, which is equal to 0.1 mm, was used to show the severe case. When the applied stress range is higher, which is more than about 230 MPa, the repetition of cyclic plastic strain is observed. In this case, the strain range at weld toe is considerably increased.

These elastoplastic strains phenomenon is the reason why fatigue crack tends to initiate from weld toe when the applied stress range increase.

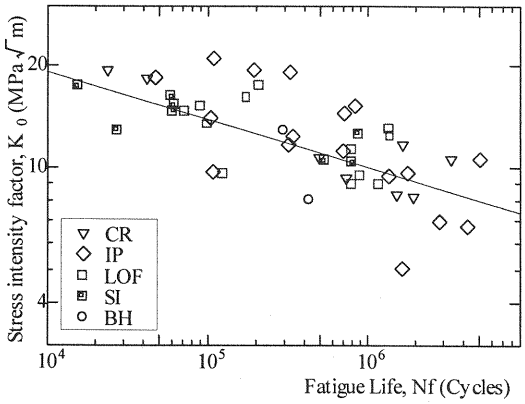

Fig.18 Initial stress intensity factor and fatigue life relationship

6. CONSIDERATION BY USING FRACTURE MECHANICS APPROACH

So far the discussion concerning fatigue behavior of the joints containing defects is performed concerning the length of the defects and the nominal stresses applied. However, as indicated in **Fig.7** that the depth of defects are quite various. The defect locations and stress distribution are also various, as shown in the previous section, see **Fig.6** and **Fig.14**, respectively. These factors are necessary to be considered in evaluating the fatigue behavior of joints containing defect. In this evaluation, only specimens failed with fatigue crack initiated from embedded defect are considered.

Initial stress intensity factor, K_0, assuming the initial crack shape[23] as shown in **Fig.2** can be defined as follows:

$$K_0 = \sigma\sqrt{\pi \cdot a} \cdot F$$

$$F = F_g \cdot F_e \cdot F_t \cdot F_h$$

where a is the half-depth of defect based on simplified crack as illustrated in **Fig.2**. F is a correction factor consisting of the effects of stress gradient, F_g, shape of crack, F_e, thickness and width of plate, F_t, as well as eccentricity of defect against central axis of plate, F_h. In order to calculate Fg factor the stress gradient is taken from the stress distribution in X-direction perpendicular to the plane of defects obtained by FEM analysis, as indicated in **Fig.15**.

Fig.18 shows the initial stress intensity factor, K_0, versus the fatigue life, Nf, relationship[23]. The regression line shown is a least squares fit to a power function. This arrangement was adopted to examine the sensitivity of weld defects. However, there is not meaning difference among the types of defects.

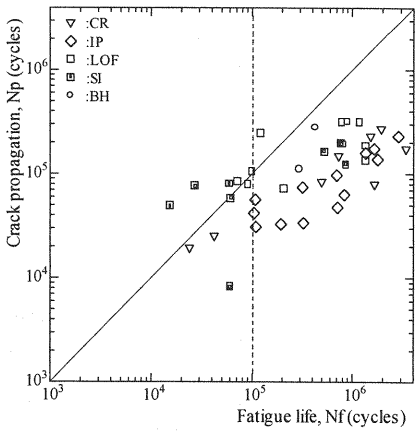

(a) The analysis considering nominal stress

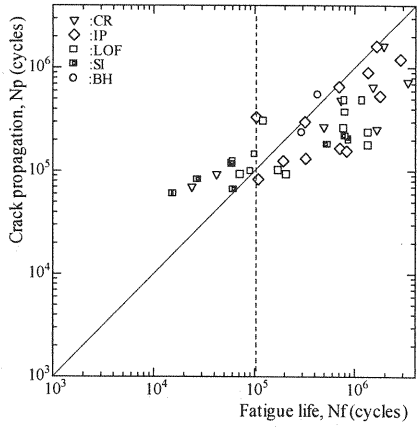

(b) The analysis considering stress distribution

Fig.19 The comparison of test results and analysis

Fatigue propagation life of specimens containing the various types of defect was carried out based on fracture mechanics. In this analysis, the dimensions of initial crack shape and correction factors used for calculating the stress intensity factors is the same as applied in the previous calculation. The modified "Paris" power law that is also recommended by the JSSC recommendation[21] is used. The formula and coefficients applied are as follows:

$$da/dN = C(\Delta K^n - \Delta K^n{}_{th})$$
$$da/dN = 0, \; if \; \Delta K < \Delta K_{th}$$

where constants $C = 1.5 \times 10^{-11}$, and $n = 2.75$ following the mean curve values recommended by JSSC[21], as well as threshold value of stress intensity factor range $\Delta K_{th} = 2.9$ (units in $MPa\sqrt{m}$).

Fig.19 shows the analysis results compared with fatigue test results to observe effect of stress

distribution on the crack propagation. The crack propagation analysis was carried out with and without the correction factor Fg.

As shown in **Fig.19(a)**, crack propagation analysis result considering nominal stress, which does not include the correction factor Fg, indicate that specimens containing CR and IP type defects have extremely conservative results compare with LOF, SI and BH defects.

On the other hand, **Fig.19(b)** shows the result by considering effect of stress distribution using the correction factor Fg. Similar to the result obtained in **Fig.18**, the analysis result shows that almost no difference among the type of defects. The differences between type of defects, which can be seen in S-N diagrams shown in **Fig.5**, depend on stress distribution near the defects.

This result indicates that the stress distribution in respect to the configuration of weld bead is necessary to be considered in the crack propagation analysis by including Fg.

Furthermore, the result shows that crack propagation analysis gives conservative result in the long fatigue life region. This is obviously due to the existence of fatigue initiation life as indicated by beach-marking test in the previous section. On the contrary, in the low cycle fatigue life the crack propagation analysis gives no conservative result.

7. TENTATIVE EVALUATION OF PERMISSIBLE DEFECT SIZE

The permissible size in length of embedded defect, 2c, is evaluated by considering the fatigue test results. The defect sizes in length are taken from the results inspected by RT. For this purpose only the fatigue test data in the region of longer fatigue life, which is more than 10^5 cycles, is considered.

To decide the permissible defect size of the joints, which is categorized as D-class, it is reasonable to use the C-class as a reference considering the safety margin. The fatigue test results are converted to the strength at $2x10^6$ cycles by applying the following relation:

$$C = N \cdot \sigma^m$$

where " m" is assumed as equal to 3. The converted fatigue test results are shown in **Fig.20** as the relation with the defect lengths.

The defect size, in which there is not smaller defect-size fail below the C-class of fatigue strength, is selected as the first criterion to decide the permissible defect-size.

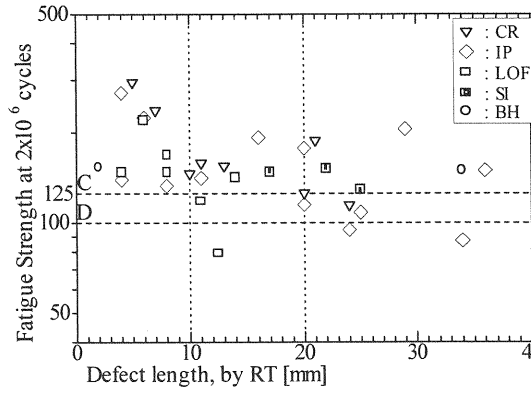

(a) Specimens failed with fatigue cracks initiated from embedded defects

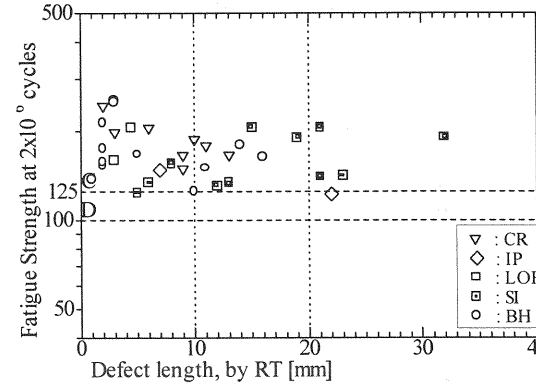

(b) Specimens failed with fatigue cracks initiated from toe

Fig.20 Relationship of defect size and fatigue strength at $2x10^6$ cycles fatigue life

In **Fig.20(a),** CR type defect clearly shows that the tendency of fatigue strength is decreased with the increasing of the defect size. For this type of defect, the defect size of about 10-mm length is considered as the permissible size. IP type of defect also shows similar tendency as CR type and the defect size of about 10-mm length is permissible defect size. LOF type of defect indicates the same tendency as CR and IP types of defect. The permissible size shown is about 10-mm. In case of SI type of defect, the data does not show a clear tendency concerning the relationship between defect size and fatigue strength. The number of data is small and no data obtained in the region of small defect size. Similar to SI type, the data of specimens with BH type defect failed from embedded defect is very few. This type of defect shows the same condition as SI type defect.

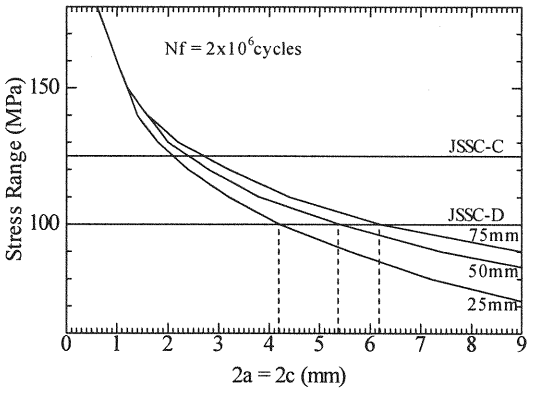

Fig.21 Permissible defect size based on fracture mechanics

Considering the ability of NDI, which is difficult to specify the type of defect, the type of the defects can not be taken into consideration. As a result of the evaluation of the data shown in **Fig.20(a)**, it can be decided the permissible defect size is 10-mm.

If there is a case that aspect ratio of cracks are close to 1, it is necessary to evaluate the permissible defect size instead of 10-mm as resulted from this evaluation.

The second criterion is the failure mode in which the specimens failed with the fatigue crack initiated from weld toe. This is usual mode, similar to the fatigue failure mode of specimens without defect. The defect size data given by specimens failed with the fatigue crack initiated from toe is useful for deciding the permissible defect size. The permissible size is considered as the largest defect length that exists in the welded joint specimens with the fatigue crack initiated from weld toe. **Fig.20(b)** shows that all specimens failed from toe have the fatigue strength of about C-class or higher. The maximum defect size of existing embedded of CR, IP, and SI types defect is larger than 10mm. Therefore, the defect length of 10-mm can be considered as a permissible defect size.

By using fracture mechanics analysis, critical defect size can be calculated. The result is as shown in **Fig.21.** By applying 100MPa stress-range for the fatigue life of $2x10^6$ cycles, the critical defect size of about 4.2-mm is obtained. The result is smaller compare to the experimental result. This result is reasonable, because the initiation fatigue life is not taken into account in the analysis. However, this value is very conservative. Therefore, further study is necessary in order to get more suitable analysis based on fracture mechanics analysis.

For larger plate thickness of the joints that have similar geometry as the 25-mm joint specimen the permissible defect sizes are a little bit larger as shown in **Fig.21**. Therefore, in case of the change of plate thickness to the thicker one there is a possibility the same value of 10-mm can be applied.

8. CONCLUSIONS

1. The fatigue strengths of butt-welded joints with defects depend on the shape as well as location of defects, and decrease with the increasing of the defect size.
2. Fatigue strengths of the joints with volumetric defects mostly failed with the crack initiated from weld toe indicating less sensitive to fatigue compare to specimens with planar defects.
3. The joint specimens containing CR and IP defects seem to have high fatigue strengths. The reason of this is that the stresses at the location of these defects are much smaller than the nominal stresses due to the geometry of weld.
4. Crack propagation analysis by using fracture mechanics present a conservative result in long fatigue life due to the existence of fatigue initiation life.
5. Defect length of 10-mm is found as the permissible size of the embedded defects of the butt-welded joints used in this study.
6. The cracks initiated from weld toe were observed more in high fatigue stresses due to weld metal over-matches base metal.

Future works: In order to generalize the permissible defect size, the following studies in consideration of different plate thickness, weld detail, welding process, as well as residual stress are needed.

ACKNOWLEDGMENT: This study is a part of collaboration research program on the assessment of butt welded joints containing various defects, which is supported by a joint research group consisting of:

- Tokyo Institute of Technology
- Public Works Research Institute, Ministry of Construction
- Japan Highway Public Corporation
- Kouzai Club (Japan Steel-mills Association)
- Japan Bridge Construction Association

This research is supported by the Grant-in-Aids for Scientific Research, Ministry of Education. The test specimens were prepared by Mr. Fumitaka Machida of Kawada Industries Inc. The authors wish to express their sincerest gratitude to all mentioned above.

REFERENCES

1) Lundin, C.D.: *Fundamentals of weld discontinuities and their significance*, W R C Bulletin, 295, Welding Research Council, New York, 1984.
2) Owens, G .W. and Cheal, B.D.: *Structural Steelwork Connections*, Butterworth, England, 1989.
3) Cary, H.B.: *Modern welding technology*, Prentice-Hall, Inc., Upper Saddle River, New Jersey, 1998.
4) Gurney, T.R.: *Fatigue of Welded Structures*, 2nd ed., Cambridge University Press, Cambridge, 1979.
5) Barsom, J.M. and Rolfe, T.R.: *Fracture and fatigue control in structures, Applications and fracture mechanics*, Prentice-Hall, Inc., Englewood Cliffs, New jersey, 1987.
6) Maddox, S.J.: *Fatigue Strength of Welded Structures*, 2nd ed., Abington Publishing, Cambridge, 1991.
7) Lawrence, F.V., Dimitrakis, S.D. and Munse, H.W.: Factors influencing weldment fatigue, ASM Handbook, vol.19, ASM International, USA, 1996.
8) Galtier, A. and Rabbe, P.: The significance of defects to fatigue behavior, International Conference on Performance of Dynamically Loaded Structures, San Francisco, CA, 1997.
9) Ishii, Y., Kihara, H. and Tada, Y.: On the relation between the non destructive testing information of steel welds and their mechanical strength, Journal of NDI, Vol. 16, No. 8, 319-345, 1967.
10) Ishii, Y. and Iida, K.: Low and intermediate cycle fatigue strength of butt-welds containing weld defect, Journal of NDI, Vol. 18, No. 10, 443-476, 1969.
11) Newman, R. P. and Gurney, T. R.: fatigue test on 1/2 in. thick transverse butt welds containing slag inclusions, first interim, British Welding Journal, 341-352, July 1964.
12) Harrison, J.D.: Basis for a proposed acceptance-standard for weld defects, Part 1: Porosity, Metal Construction, 99-107, March 1972.
13) Harrison, J.D.: Basis for a proposed acceptance-standard for weld defects, Part 2: Slag inclusions, Metal Construction, 99-107, March 1972.
14) Miki, C., Okukawa, A., Ooe, S. and Yasui, S.: Fatigue strength of corner welds of truss chords containing blowholes, Structural Eng./Earthquake Eng.Vol. 9, No. 2, 109s-116s, July 1992.
15) Miki, C., Mori, T., Sakamoto, K. and Sasaki, T.: An analysis of fatigue crack growth from blowholes in longitudinal welded joints, Structural Eng./Earthquake Eng.Vol. 4, No. 2, 289s-297s, October 1987.
16) Stig, W. and Agnar, K.: *Significance of defects, Fatigue Handbook, Offshore Steel Structures*, Tapir Forlag,Norge, 1985.
17) Draft of IIW Recommendation: *Application of an engineering critical assessment in design*, fabrication and inspection to assess the fitness for purpose of welded structures, SST-1141-89, 1989.
18) Gordon, J.R.: Fitness-for-Service Assessment of Welded Structures, ASM Handbook, vol.6, ASM International, USA, 1993.
19) The Japan Welding Engineering Society: *Method of assessment for flaws in fusion welded joints with respect to brittle fracture and fatigue crack growth*, WES 2805-1997, 1997.
20) The International Institute of Welding: *IIW Fatigue recommendation*, XIII-1539-96/XV-845-96, May 1996.
21) The Japanese Society of Civil Engineering: *Fatigue design recommendations for steel structures* (English version), December 1995.
22) Barsom, J.M. and Vecchio, R.S.: Fatigue of welded components, WRC Bulletin 422, 1997.
23) Gill, S.J. et al.: Fatigue behavior of 5Ni-Cr-Mo-V steel weldments containing fabrication discontinuities, ASTM STP 945, 1025-1049, 1988.

(Received January 14, 2000)